Estuarine, Coastal and Shelf Science 149 (2014) 294–301

Contents lists available at ScienceDirect

Estuarine, Coastal and Shelf Science

journal homepage: www.elsevier.com/locate/ecss

Modelling alongshore flow in a semi-enclosed lagoon strongly forced by tides and waves

Torbjørn Taskjelle [a, 1], Knut Barthel [a, *], Kai H. Christensen [b], Noca Furaca [c], Tor Gammelsrød [a], António M. Hoguane [c], Bilardo Nharreluga [c]

[a] Geophysical Institute, University of Bergen, Bergen, Norway
[b] Research and Development Department, Norwegian Meteorological Institute, Oslo, Norway
[c] Escola Superior de Ciências Marinhas e Costeiras, Quelimane, Mozambique

ARTICLE INFO

Article history:
Received 18 March 2014
Accepted 6 September 2014
Available online 26 September 2014

Keywords:
lagoon circulation
waves and mass transport
1D model

ABSTRACT

Alongshore flows strongly driven by tides and waves is studied in the context of a one-dimensional numerical model. Observations from field surveys performed in a semi-enclosed lagoon (1.7 km×0.2 km) outside Xai-Xai, Mozambique, are used to validate the model results. The model is able to capture most of the observed temporal variability of the current, but sea surface height tends to be overestimated at high tide, especially during high wave events. Inside the lagoon we observed a mainly uni-directional alongshore current, with speeds up to 1 ms^{-1}. The current varies primarily with the tide, being close to zero near low tide, generally increasing during flood and decreasing during ebb. The observations revealed a local minimum in the alongshore flow at high tide, which the model was successful in reproducing. Residence times in the lagoon were calculated to be less than one hour with wave forcing dominating the flushing. At this beach a high number of drowning casualties have occurred, but no connection was found between them and strong current events in a simulation covering the period 2011–2012.

1. Introduction

Reefs are common features along the coasts of the tropical oceans and often define semi-enclosed areas that can be densely populated. This is because such lagoons define particular ecosystems subject to fisheries, development of tourist industries, and in recent years also fish-farming. Therefore it is of interest to know the circulation in such areas to secure that the water quality may sustain the increased sewage discharges from growing settlements, the environmental impact of near-shore constructions and increased industrial activities. Coastal erosion is also of major concern, so it is important to study ocean currents, tides, waves and wind influencing erosion processes. An illustrative example is the study of Sandy Bay, Australia (Taebi et al., 2011).

In this paper we investigate the current dynamics at the beach of Xai-Xai, southern Mozambique. At Xai-Xai there is a fringing reef running parallel to the coast defining a lagoon about 1.7 km long and up to 200 m wide, see Fig. 1. The lagoon is almost closed in the west, and the major openings are found in the eastern end. The reef itself is only about 20 m wide and very regularly shaped, resembling the remains of a man made jetty. The tidal amplitudes in the area range from 0.5 m during neap and up to 1.5 m at spring tide (Sete et al., 2002). The uppermost level of the reef has a more or less constant height and is always submerged during high tides. At low tide the reef is always above sea-level. Waves may induce a mass flux across the reef even when the water level is below the top of the reef (Sibul, 1955). The water exits the lagoon mainly through the gaps in the eastern end.

Several studies of wave driven flow across reefs and wave driven circulation have been made. Early work includes Munk and Sargent (1954), who looked at circulation within a Pacific atoll. Gourlay (1996) performed laboratory experiments, seeking dimensionless parameters relating wave set-up on the reef and wave driven flow across the reef, which Kirugara et al. (1998) applied to develop analytical models for the Bamburi Lagoon, Kenya, see also

* Corresponding author. Department of Physics and Technology, University of Bergen, Norway.
E-mail address: Knut.Barthel@gfi.uib.no (K. Barthel).
[1] Presently at Department of Physics and Technology, University of Bergen, Norway.

http://dx.doi.org/10.1016/j.ecss.2014.09.008

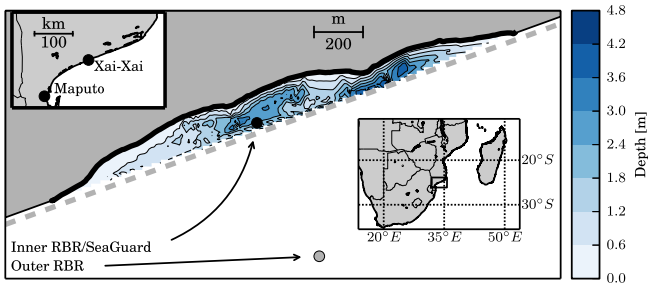

Fig. 1. Map showing a GPS track along the shoreline (thick black line) from October 2013, and bathymetry measured by echo sounder in October 2011. Instrument positions from survey in October 2012 are indicated. The dashed grey line indicates the approximate position of the reef. The insets show the location of Xai-Xai in southern Africa.

Angwenyi and Rydberg (2005). Lowe et al. (2009) defined an idealised model for a system with a reef and a lagoon, applying it to Kanehoe Bay, Hawaii. They related cross-reef flow to wave setup on the reef. Based on field experiments (Taebi et al., 2011) a two-way coupled circulation and wave model, investigating the circulation in a fringing reef, was developed by Taebi et al. (2012). Field studies at Bora Bay, Miyako Island by Kraines et al. (1998) showed that the cross-reef flow did not follow the tidal cycle, but was low at low tide and also had a local minimum at high tide. They explained the minimum at low tide by a blocking effect by the reef, and the corresponding minimum at high tide was found to be related to a reduced radiation stress gradient due to less wave breaking when the water level at the reef was high. Taebi et al. (2011) found the same sub-tidal oscillation of the current system at Sandy Bay, Australia. The importance of wave setup has been addressed by several of the above mentioned studies, see also Lowe et al. (2010). Antuono et al. (2007) developed 2D analytical models for alongshore circulation due to waves at a beach, while Stockdon et al. (2006) performed 10 field experiments to study wave setup, swash and run-up under various conditions.

The model efforts mentioned above all concentrate on the dynamics of wave and tide induced transports across the reefs which typically are several hundred metres wide. At Xai-Xai the reef is only about 20 m wide, and we have formulated the transports across the reef as functions of the offshore wave state and water level. We have developed a 1D model for the alongshore flow inside the lagoon. Our goal was to identify the main driving forces determining the time development of the current, as well as the alongshore variability. The intention here was to investigate if a model based on simple conservation laws could reproduce the main observed dynamics. We present also a few short (~1 day) observation series of current, water level and waves in the area.

This study was also motivated to see if there were any connections between strong current events and the large number of casualties due to drowning reported at this beach. A two years long model simulation is performed and the results are compared with data of drowning incidents.

In Section 2 we describe the field experiments at Xai-Xai beach. The model is developed in Section 3, and in Section 4 we present the measurements and a model run with idealised forcing. In Section 5 we force the model with realistic parameters, measured and modelled, and the output of the model is compared with observations. Section 6 contains some concluding remarks.

2. Field experiments

Field experiments were designed to obtain measurements of the parameters believed to be essential for the lagoon dynamics, such as sea level and waves inside and outside the lagoon, currents and bathymetry inside the lagoon. During a field survey in Xai-Xai in October 2011 bathymetric data inside the lagoon was collected, using a Garmin echo sounder. As the depth soundings were done over three days, at various times of the day, we adjusted the values by subtracting a modelled tidal amplitude from the TPXO.7 tidal model (Egbert and Erofeeva, 2002). The adjustments made were up to ±0.4 m. A GPS track along the beach (thick black line in Fig. 1) that was recorded in October 2013 was used to define the land side of the lagoon, where the depth is zero. The GPS track and echo depths were interpolated to a regular and rectangular grid, to get the bathymetry shown in Fig. 1.

A second field survey was performed in Xai-Xai in October 2012 close to spring tide (Christensen et al., 2013). Point measurements of current velocity inside the lagoon (Fig. 1) were obtained using an Aanderaa SeaGuard moored at a depth of about 1 m below surface. The instrument contains a Doppler Current Sensor with high accuracy (0.15 cm s^{-1}).

We used two TWR-2050 pressure sensors from RBR to measure both the varying sea surface height due to tides, as well as wave parameters. Waves were measured in 'bursts', with the instrument recording 2048 samples at 2 Hz, repeating this procedure every 20 min. Tidal averaging was done every five minutes. The accuracy of the pressure sensor is 0.05% of the full scale, which in our case corresponds to about 1 cm of water. We mounted one sensor inside the lagoon, on the same mooring that held the current meter ('inner RBR', black dot in Fig. 1), while the other was mounted about 600 m outside the reef ('outer RBR', grey dot in Fig. 1).

A Lagrangian drifter buoy with a GPS unit was used to measure surface currents. The drifter was equipped with a Garmin DC40 transducer, and a handheld Garmin Astro 440 was used to log the position of buoy. The transducer was set to measure every five seconds, but several data points were not logged, possibly due to communication issues between transducer and the handheld unit, giving an irregular sampling interval.

In addition to the field observations, wave data from the ERA-Interim reanalysis (Dee et al., 2011) for January 1, 2011 to December 31, 2012 was obtained for a location about 50 km east of Xai-Xai. The TPXO.7 tidal model was run for the same location, creating a simulated time series of sea surface height for the same period, 2011–2012.

Comparisons between modelled data from ERA-I and TPX and data from the outer RBR generally show a good agreement, indicating that the modelled data is representative for Xai-Xai, cf. Fig. 2.

3. Model

A simplified model for the circulation in the lagoon at Xai-Xai is defined, where constant density is assumed and Coriolis forces are neglected. Fig. 3 shows a schematic of the system. The x-axis is placed parallel to the reef, with positive direction east-northeast (cf. Fig. 1). The model domain is closed on the left end, has a length of 1700 m and a width B varying in the range 80–200 m. The reef is about 20 m wide and defines a straight line. Inside the reef is an alongshore current $u(x,t)$ and sea surface height $\zeta(x,t)$. Forcing the system inside the lagoon is the sea surface height outside the lagoon $\eta(t)$ and a transport of water across the reef $V(x,t)$, caused by wave and a pressure gradient due to cross-reef sea level differences. Inside the lagoon, most waves have dissipated, and we ignore second-order wave effects, that is, setup/setdown inside and outside of the lagoon, or the excitation of low frequency (infragravity) waves (e.g., edge waves). Fig. 3b shows a cross section of the model lagoon. Sea surface heights are given as the deviation from a mean sea level. Table 1 contains a list of the parameters used in the model.

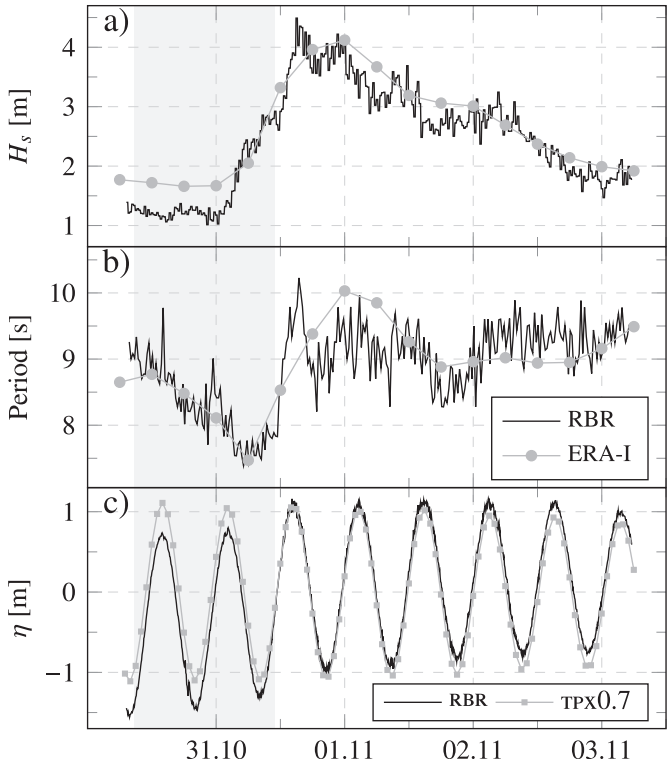

Fig. 2. Comparison of measurements by RBR with ERA-Interim and the TPXO.7 tidal model for October–November 2012. a) shows significant wave height (ERA-I), b) shows mean wave period (ERA-I) and c) shows tidal elevation (TPX). The grey shading indicates the period when concurrent measurements were made inside the lagoon, i.e. that displayed in Fig. 6.

3.1. Conservation of momentum

By assuming hydrostatic balance, we can write the alongshore pressure gradient term in terms of the interior water level, ζ, i.e. $-g(\partial\zeta/\partial x)$. The frictional term is parameterised as being proportional to the current speed, i.e. $-ru$ (Rayleigh friction, Weber et al. (2007)), where r is a coefficient for bottom friction, here chosen as 10^{-3} s^{-1}.

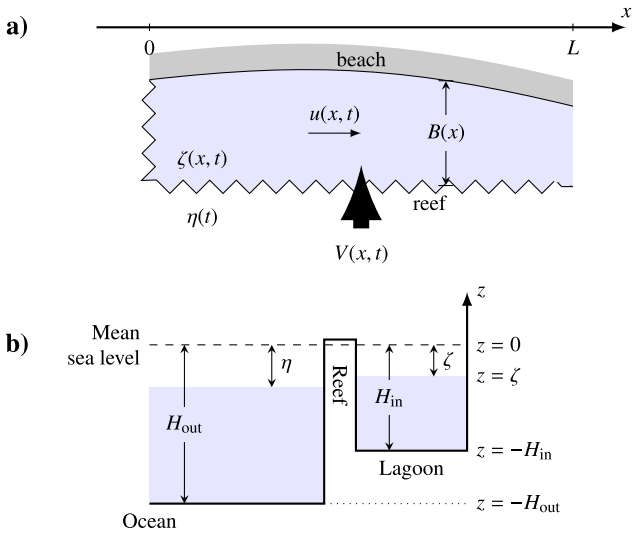

Fig. 3. Schematic view of the system. Panel a) shows variations in x, while panel b) shows a cross section of reef, indicating different depths for a situation near low tide.

Table 1
Parameters and variables of the model.

Name	Description
L	Length of lagoon
B	Width of lagoon
u	Alongshore current velocity inside the lagoon
ζ	Sea-level inside the lagoon, deviation from mean
η	Sea-level outside the lagoon, deviation from mean
H_{in}	Mean water depth inside the lagoon
H_{out}	Mean water depth outside the lagoon
H_s	Significant wave height
V	Cross-reef volume transport per unit length
V_{w}	Contribution to V by waves
V_{sld}	Contribution to V by cross-reef sea level difference
ε	Coefficient for wave-driven cross-reef volume transport
h_b	Lower limit of η for wave driven inflow
h_t	Limit of η for maximum inflow
λ	Coefficient for cross-reef volume transport driven by sea level differences
h'_b	Lower limit for pressure driven cross-reef flow
h'_t	Transitional level for cross-reef flow
r	Rayleigh friction coefficient

The momentum equation for the x-direction becomes (e.g. Marshall and Plumb, 2008).

$$\frac{\partial u}{\partial t} + u\frac{\partial u}{\partial x} = -g\frac{\partial \zeta}{\partial x} - ru, \tag{1}$$

Experiences with drifter experiments indicate that the current usually was eastwards even during episodes with strong winds towards west, so wind effects are neglected in the model.

3.2. Conservation of volume

Considering a small cross-section control volume, changes in the sea level within the control volume will be a result of the balance between the flow into or out of the sides of the control volume. Fig. 4 shows a top view of such a control volume of the lagoon having width Δx. The fluxes into this control volume are:

$$\begin{aligned} I:&\quad [(\zeta + H_{\text{in}})Bu](x) \\ II:&\quad -[(\zeta + H_{\text{in}})Bu](x + \Delta x) \\ III:&\quad V(x)\Delta x \end{aligned} \tag{2}$$

The change of volume during a period Δt is $(I + II + III)\Delta t$. As the model depth is independent of width, the change of volume is also given by $B\Delta x\Delta\zeta$. Equating the two expressions for change of volume and dividing by $B\Delta x\Delta t$ we get, in the limit $\Delta t, \Delta x \to 0$,

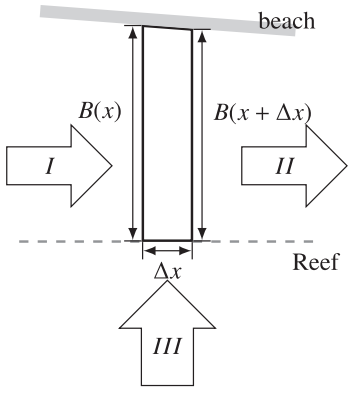

Fig. 4. Schematic illustration of the terms in continuity equation. The schematic shows a control volume in the lagoon. The change in volume is determined by what flows into it from the left (*I*), what flows out on the right (*II*) and what comes across the reef (*III*).

$$\frac{\partial \zeta}{\partial t} = \frac{1}{B}\left[V - \frac{\partial}{\partial x}\left[(\zeta + H_{\text{in}})Bu\right]\right]. \tag{3}$$

We write $V = V_{\text{w}}(t) + V_{\text{sld}}(x,t)$, where V_{w} represents the Stokes transport by incoming waves and is assumed homogeneous along the reef, and V_{sld} represents pressure-gradient driven flow due to a cross-reef sea level difference.

The former is obtained from the vertically integrated Stokes drift (Longuet-Higgins, 1953), which for a monochromatic wave is given by

$$M = \int_{-H_{\text{out}}}^{0} \frac{a^2 \omega k \cosh\left[-2k(z + H_{\text{out}})\right]}{2\sinh^2(kH_{\text{out}})}\, \text{d}z, \tag{4}$$

where a is the wave amplitude, k is the wave number, $H_{\text{out}} = 17$ m is the depth of the water column, ω is the angular wave frequency, and z is depth. The wave number k can be found through the dispersion relation for waves, $\omega^2 = gk\tanh(kH_{\text{out}})$. The incoming waves are predominantly swell and we will approximate the Stokes transport using the assumption that $a = H_s/2$, where H_s is the measured or modelled significant wave height, i.e. we assume that the waves are monochromatic. Introducing a dimensionless scaling factor ε and a dependency on the sea level η, we assume that the wave-induced transport can be written

$$V_{\text{w}} = \varepsilon M \cdot F_{\text{w}}(\eta), \tag{5}$$

where the limiting function $F_{\text{w}}(\eta)$ is given by

$$F_{\text{w}}(\eta) = \begin{cases} 1, & \eta > h_t, \\ \left(\dfrac{\eta - h_b}{h_t - h_b}\right)^2, & h_b \le \eta \le h_t, \\ 0, & \eta < h_b. \end{cases} \tag{6}$$

The limits h_b and h_t determine the sea level necessary to get flow across the reef due to wave forcing, and the level where additional rise gives no added effect, respectively. The quadratic dependence in Eq. (6) reflects the increasing number and size of openings in the reef, and that more mass is transported by the waves when the sea level increases.

The second term, V_{sld}, is proportional to the cross-reef mean sea level difference and a similar limiting function as Eq. (6):

$$V_{\text{sld}} = \lambda \cdot (\eta - \zeta) \cdot F_{\text{sld}}(\overline{\zeta}), \tag{7}$$

where the coefficient λ has units m s^{-1}, and

$$F_{\text{sld}}(\overline{\zeta}) = \begin{cases} 1 + \dfrac{\overline{\zeta} - h_t'}{h_t' - h_b'}, & \overline{\zeta} > h_t', \\ \left(\dfrac{\overline{\zeta} - h_b'}{h_t' - h_b'}\right)^2, & h_b' \le \overline{\zeta} \le h_t', \\ 0, & \overline{\zeta} < h_b', \end{cases} \tag{8}$$

with $\overline{\zeta} = \max(\eta, \zeta)$. The gradual transition defined by F_{sld} reflects that the reef is not a smooth block, but has gaps, so that for a sea level close to the lower limit h_b' just a little water can pass through, while for a high enough sea level there are no obstacles to the flow. When the sea level is higher than the top of the reef, defined by h'_t, the size of cross-reef transport is determined not just by the pressure gradient, but also by the height of the water above the top of the reef, with higher sea level allowing for higher transport, due to increased area. The term $1 + (\overline{\zeta} - h'_t)/(h'_t - h'_b)$ is defined to account for this effect.

A final modification is to give the width at the easternmost end of the lagoon a linear dependency on η. This is to account for the fact that the width of the eastern outlet increases with increasing sea level.

3.3. Boundary conditions

To solve Eqs. (1) and (3), appropriate boundary conditions must be given. As the western edge of the model lagoon is closed, the velocity at this boundary must be zero. Furthermore, the sea level at the opening of the reef at the eastern end must be the same as the sea level outside the reef. Hence, we get

$$u(x = 0, t) = 0, \tag{9}$$

$$\zeta(x = L, t) = \eta(t). \tag{10}$$

3.4. Discretisation

We define $t = n\Delta t$ and $x = j\Delta x$. For the discretisation of Eqs. (1) and (3), staggering of u an ζ in both space and time is applied, with u staggered a half time step after, and a half grid length to the right of, ζ. A forward-backward scheme is used, the forward step is used on the equation for $\partial\zeta/\partial t$, and a backward step for $\partial u/\partial t$. In addition, the frictional term in the momentum equation is placed at time $n + 1$, giving the following finite difference equations:

$$\begin{aligned} \frac{\zeta_j^{n+1} - \zeta_j^n}{\Delta t} = \frac{1}{B_{2j-1}}\Bigg[V_j^n - \frac{1}{\Delta x}\Bigg(&\left[0.5\left(\zeta_{j+1}^n + \zeta_j^n\right) + H_{\text{in}}\right] B_{2j} u_j^n \\ &- \left[0.5\left(\zeta_j^n + \zeta_{j-1}^n\right) + H_{\text{in}}\right] B_{2j-2} u_{j-1}^n\Bigg)\Bigg], \end{aligned} \tag{11}$$

$$\frac{u_j^{n+1} - u_j^n}{\Delta t} = -u_j^n \frac{u_{j+1}^n - u_{j-1}^n}{2\Delta x} - g\frac{\zeta_{j+1}^{n+1} - \zeta_j^{n+1}}{\Delta x} - r u_j^{n+1}. \tag{12}$$

Due to the staggered grid, ζ is linearly interpolated to u-points in the continuity equation, Eq. (11). For the width B, the grid length is $\Delta x/2$, making interpolation unnecessary as B is defined in both ζ and u points.

For the first grid cell, the last term in Eq. (11) and the second term in the numerator of the advection term vanishes because of the boundary condition Eq. (9). For the last grid cell, $\zeta_{j+1} = \eta$, due to the boundary condition, Eq. (10). Also in the last cell, $\partial u/\partial x$ in the advection term is approximated by a one sided difference, rather than a centred difference. Hence, u_{j+1} is not needed. Table 2 has the values used for Δx and Δt.

4. Results

4.1. Observations

GPS drifters has been used several times to provide information about the alongshore variability of the flow, and all experiments so far have shown that the flow direction is consistently towards the east, and is primarily in the alongshore direction. A slow onshore drift component could often be observed, possibly caused by wave-

Table 2
Model parameters used for the simulations (Figs. 7–9).

dx	dt	ε	λ	r
50 m	1 s	2.8	1	0.001 s^{-1}
h_b	h_t	h_b'	h_t'	
−0.7 m	0.4 m	−0.5 m	0.4 m	

induced drift in the upper part of the water column or wind drag. Nevertheless, the drifter observations lend support to our assumption of a closed boundary at the western end of the lagoon, and also the choice of a 1D model for the main circulation. Fig. 5 shows the tracks from three deployments of a drifter in the lagoon at Xai-Xai Beach from October 31, 2012. The mean speed for these drifters were between 0.6 m s^{-1} and 0.8 m s^{-1}, which is a little higher than the current speed measured by the SeaGuard at the same time. Similar results were also observed in drifter experiments at neap tide during three days in October 2011 (not shown), with mean drifter speeds generally lower, at around 0.3 m s^{-1}.

Fig. 6 shows measurements by the sea level recorders (RBR) from October 2012 inside (ζ) and outside (η) the lagoon, as well as the alongshore current speed obtained with the SeaGuard inside the lagoon and the significant wave height outside the lagoon. The tide inside and outside of the lagoon are similar, although at the end of the time series the sea level inside the lagoon is 15–20 cm higher than on the outside (Fig. 6b).

The significant wave height outside the reef remains almost constant at about 1.2 m until about 03:00 on October 31 when the value rises to about 2.9 m because of the increasing incoming swell connected to a passing low pressure system.

On October 30 the alongshore velocity (u) increased from zero in the beginning of the time series and obtained a local maximum around 11:00. Then it was reduced to a local minimum during high tide at 14:00 before it increased to a second local maximum at about 17:00. At low tide the current was again reduced to around zero before it started to increase again with a tendency for a local maximum before high tide and the absolute maximum (0.7 m s^{-1}) after the high tide. However, it did not return to zero at low tide when the significant wave height remained above 2 m.

4.2. Idealised model run

A series of model runs were made to estimate the model parameter values. Fig. 7a shows a simulated time series from the model. Forcing this simulation is a constant wave field with a significant wave height of 1.5 m and a wave period $T = 2\pi/\omega$ of 10 s, and a sinusoidally varying sea surface height with the period of the M_2 tide and an amplitude of 1 m. The model settings are as given in Table 2. The simulated time series is taken from a grid point close to the centre of the lagoon, indicated by the dotted line in Fig. 7b, which shows the spatial variation of the model.

As the tide rises the current speed increases from the time just after η passes the lower limit h_b until just after it has passed the upper limit h_t. A small decrease of u follows as the sea level continues rising, and a similar increase at the start of ebbing, lasting until η has passed h_t again.

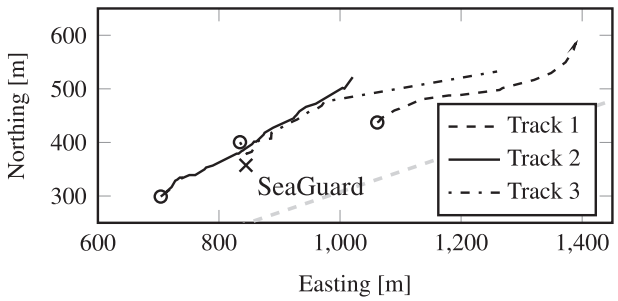

Fig. 5. Tracks of three deployments of a surface drifter from the morning of October 31, 2012, between 09:30 and 11:00, each lasting about 10 min. The circles indicate the start of the tracks, the dashed grey line is the approximate location and orientation of the reef. Distances are relative to a point in the western end of the lagoon, roughly where $x = 0$ in the modelled lagoon. See Fig. 1 for bathymetry.

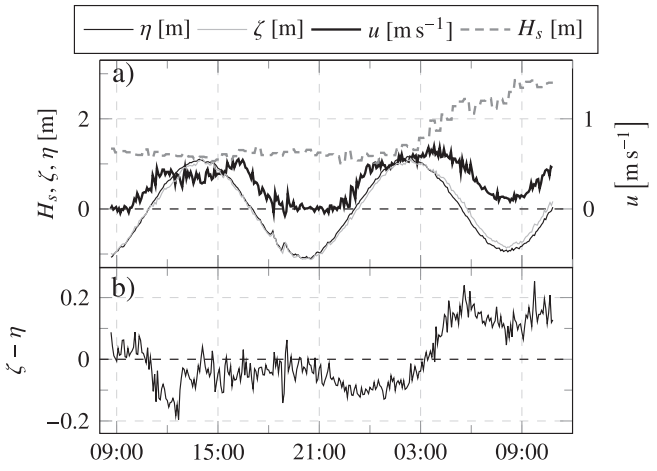

Fig. 6. a): Measured current speed, sea surface heights and significant wave height from October 30–31, 2012. η and H_s are measured by the outer RBR (cf. Fig. 1), ζ and u are measured inside the lagoon, by the inner RBR and SeaGuard, respectively. Note the different scale for u. b): Measured sea level difference between the inside and the outside of the lagoon.

Fig. 7b shows the spatial variation of the model for two different times, near low tide and near high tide, as indicated by the vertical dotted lines in Fig. 7a. The top panel shows the difference $\zeta - \eta$, between the interior and exterior sea levels. For this specific case the difference is up to about 20 cm at $x = 0$, near high tide, and much less near low tide. ζ approaches η closer to the opening, creating a strong gradient. The middle panel shows the current speed, demonstrating that it is generally stronger closer to the opening in the eastern end, due to the narrowing of the lagoon, and the increased mass flux. Between about 1400 m and 1500 m there is a reduction in the current speed, which coincides with the widening of the lagoon here. The bottom panel shows the width of the model lagoon, which is closed at $x = 0$ m.

5. Discussion

5.1. Model behaviour

The flattening and slight dip in the current speed seen around high tide in Fig. 7a seem to be caused by a combination of two effects. Firstly, the wave forcing will be constant as long as $\eta > h_t$, so that the wave induced cross-reef volume flux stops increasing further. When the outer mean sea level rises above this limit, the acceleration ceases and the constant volume flux maintains a constant pressure gradient inside the lagoon which is balanced by friction. Secondly, the rising sea level will give a larger cross-sectional area, allowing for the same volume transport with a lower current speed. This explains the small reduction in current speed just before maximum tide. The small increase in current speed seen just after the maximum tide is caused by the same process. Reduced cross-sectional area requires a higher current speed to maintain the same volume transport. Similar current variability have been reported earlier, e.g. Kraines et al. (1998) and Taebi et al. (2011). Kraines et al. (1998) explained this being due to smaller radiation stress gradient at high tide when less wave breaking occur.

5.2. Simulation using field observations

Fig. 8 shows the measurements from inside the lagoon, along with results of a simulation where measurements of η and H_s from the outer RBR (see Fig. 6) were used to force the model. The

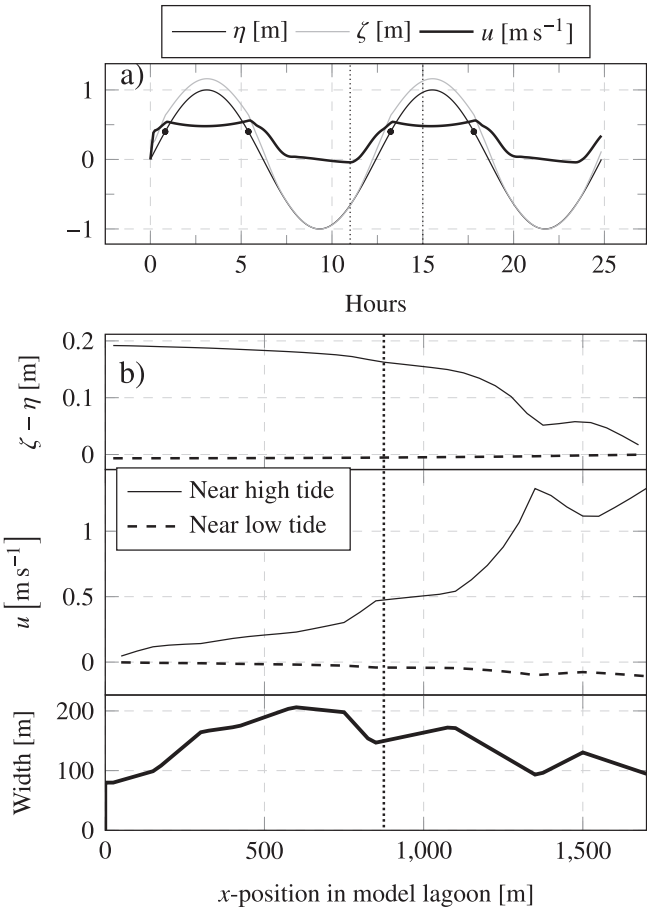

Fig. 7. a): Time series from an ideal case, with the model forced by constant, prescribed wave field, and sinusoidally varying sea surface height, with a period like that of the M_2 tide. The dotted vertical lines indicate the times used in panel b). The black dots indicate the moments where η crosses h_t. b): The spatial variation in the model. The upper panel shows the difference between the interior sea level ζ and the exterior sea level η, the middle panel shows the current speed. The spatial variation for two points in time are shown, one near low tide, one near high tide. These points in time are indicated by the dotted vertical lines in a). The lower panel shows the width of the model lagoon. The dotted black line indicate the grid point used for the simulated time series in Figs. 7a, 8 and 9.

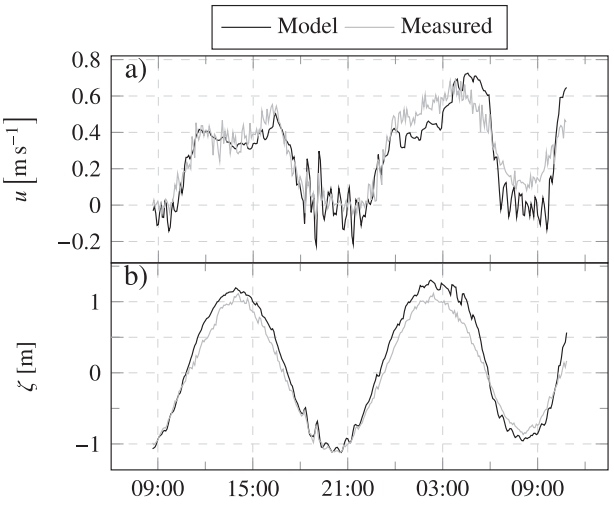

Fig. 8. Model forced with measurements from the outer RBR, compared with measurements by SeaGuard and inner RBR. For October 30–31 2012. a) shows current speed, b) shows sea surface height.

modelled time series is from the same grid point used in Fig. 7a, that is, the one closest to where the inner RBR and SeaGuard were deployed. To let the model adjust from the initial values, the time series were padded. The outer sea surface height was padded with a sine wave, the significant wave height and mean wave period with a constant equal to the first measured value. Table 2 gives the parameter settings used for the simulation.

The current speed, shown in Fig. 8a, is modelled very well for the first part of the time series, including the small dip near the first high tide. During the last third of the simulation the fit is not as good. Between 03:00 and 06:00 on Oct 31 there is a peak in the simulated u that is higher and delayed compared to the measurements, which is caused by the rapid increase of wave height seen from around 03:00 (Fig. 6), giving a larger model flow of water into the lagoon, as the Stokes drift depends on the square of wave amplitude (cf. Eq. (4)).

After the peak the deceleration seen in the model is much higher than that in the measurements, due to the higher current speed around 05:00, and that the limiting function reduces the wave forcing to zero during ebbing, effectively reducing u to near zero. Similarly, the acceleration for the last hour of the simulation is much larger than what the measurements show. Around low tide the modelled current speed fluctuates around zero, which may be caused by a standing wave. The measurements show a similar behaviour during the low tide on Oct 30, but on Oct 31 the flow is consistently eastwards, never reaching zero.

The sea surface height, Fig. 8b, is modelled well around low tide, but the model tends to overestimate it around high tide. This is particularly evident just after 03:00 on Oct 31, when the difference between model and measurements is at most about 0.4 m. This large difference coincides with the peak in the current speed, and has the same cause, that is the increase in significant wave height, which starts between midnight and 03:00. It appears that the model does not behave that well for large significant wave heights. However, the observed time series are rather short which limits firm conclusions.

The underestimation of ζ at the last low tide is likely caused by the measured outer sea surface height, which is a boundary condition for the model, being lower than that inside, cf. Fig. 6.

One should also note that the modelled current speed is a mean value for the entire width of the lagoon, which has no varying bathymetry, other than the changing width. The depth of the model lagoon is set to the mean depth measured by the RBR – about 2.7 m – which is a relatively deep spot in the lagoon (cf. Fig. 1). The measurements are point measurements, and there will likely be variations across the lagoon. That the model depth is relatively large, combined with no u-variations perpendicular to the beach, may give larger volume transport in the model lagoon than in nature, when current speeds are similar. Hence, a modelled current speed that is lower than the measured one may be more appropriate, when considering the volume transport.

A final point to consider is that for the large wave heights seen at times (see Fig. 2) non-linear wave dynamics that are ignored in our model may be important, for instance that the outside water level depends on the incoming waves through e.g. radiation stresses. The potential impact for modelled sea level difference is unclear, but we note that in general non-linear wave effects would play a greater role for increasing H_s. For example, Stockdon et al. (2006) reports wave setup values typically of $O(1\text{ m})$ for $H_s \sim 2$ m.

5.2.1. Residence time

Following Taebi et al. (2011) we define residence time as

$$\tau = \frac{V}{Q}, \tag{13}$$

where V is the total volume of the lagoon and Q is the modelled cross-reef flow into the lagoon averaged over one tidal period. This

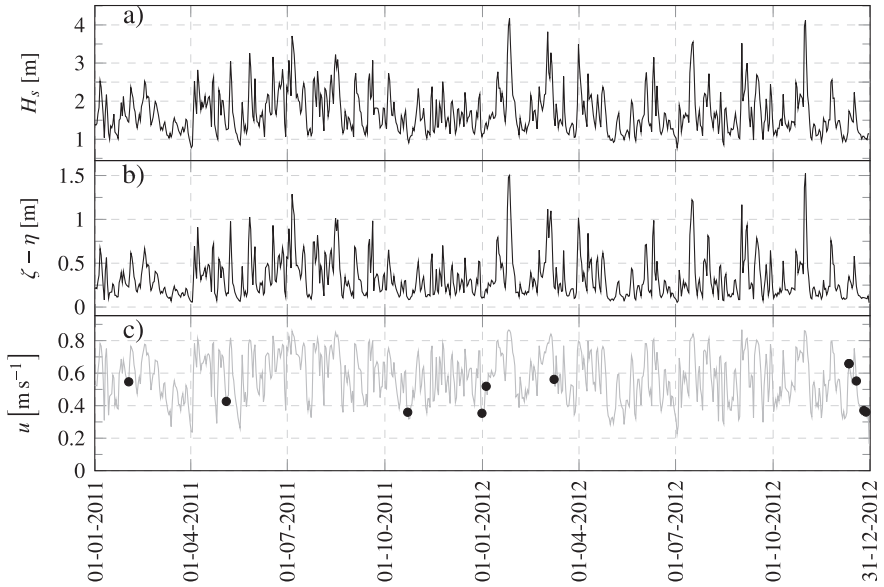

Fig. 9. Daily maxima of a) significant wave height (H_s) from ERA-Interim; b) modelled $\zeta - \eta$ and c) modelled u, from a two year long simulation where modelled data from ERA-Interim and TPXO.7 was used to force the model. The black dots indicate dates where accidents have been reported at Xai-Xai.

gives a residence time of less than one hour, indicating a very efficient flushing of the lagoon. Another definition of τ based only on tidal transports, known as the "tidal prism method" (Kraines et al., 1998), is given as

$$\tau = \frac{\text{mean depth}}{\text{tidal range/tidal period}}, \tag{14}$$

and gives a residence time of about 16 h for a tidal range of 2 m, consistent with spring tide. This shows that the wave transport is in our case more important for flushing lagoons, see e.g. Prager (1991). Flushing times of a few hours were also found at Bora Bay (Kraines et al., 1998) and at Sandy Bay (Taebi et al., 2011).

5.3. Two-year simulations

In order to test the model for a range of realistic scenarios, it was forced with modelled data for a two year-period, starting January 1, 2011. Sea surface height was obtained from the TPX tidal model (Egbert and Erofeeva, 2002), wave parameters from the ERA-Interim reanalysis (Dee et al., 2011).

Fig. 9 shows time series of daily maxima from the model simulation, as well as for the significant wave height from ERA-Interim (9a). Fig. 9b shows the difference between modelled interior sea level ζ, and the exterior sea level η used to force the model, while Fig. 9c shows u. The same grid point as in Fig. 8 was used. One would expect that the sea level inside the lagoon, ζ, was about the same as that outside, η. We have seen from Fig. 8 that the model does tend to overestimate ζ. Fig. 9b demonstrates that for some conditions the overestimation becomes very large, with differences up to about 1.5 m. Comparing with Fig. 9a, we see that these events occur on days with large significant wave heights. Although the data are limited, Fig. 8 indicates that for significant wave heights above 2–2.5 m the model does not behave very well, possibly because some non-linear effects are neglected. Of the two years of data from ERA-Interim, about 17% have H_s above 2 m, and about 5% above 2.5 m. Apparently, the model does not allow for a quick enough draining of the lagoon, causing too much water to pile up. One could compensate for this by increasing λ, the coefficient for the cross-reef flow driven by sea level differences, but this would also cause a general reduction of modelled current speed.

While the tides have a great influence on the system, no clear spring-neap cycle can be seen in Fig. 9c. This is because the wave forcing reaches its maximum when the sea level is above h_t (the upper limit in Eq. (6)), and the highest current speeds are seen when $\eta \approx h_t$ (cf. Fig. 7). For the sea level to have a significant impact on the highest current speed seen during a day, the sea level at high tide would have to be below 0.4 m above the mean, the value chosen for h_t. Therefore, the variability in the significant wave height is more important for determining the strongest current seen in any given day.

Indicated with black dots in Fig. 9c are dates when accidents have been reported at the beach. None of them are on days with particularly high current speeds. Hence, it does not appear that accidents are related to days with a stronger than normal alongshore current.

6. Conclusions

Outside Xai-Xai, southern Mozambique, there is a 1.7 km long lagoon defined by a reef running parallel to the beach. The reefs defining such lagoons are typically several hundred metres wide, but outside Xai-Xai it is only about 20 m wide, and very regularly shaped defining a straight line, see Fig. 1. The main opening of the reef is found in the east-northeastern end of the reef. The main currents inside the reef have been observed to be unidirectional towards east-northeast, independent on wind direction.

Here we present measurements of water level and the state of the waves inside and outside the reef, and currents inside the reef using both Lagrangian and Eulerian current meters. The experiments were conducted during spring tide, and the tidal range was 2.2 m with a dominating semi-diurnal period. Significant wave heights outside the reef were measured in the range 1.1–4.4 m with dominating periods typical for swell (8–10 s). The current minimum was observed around low tide, but the current maximum occurred during flooding and ebbing, see Fig. 6. Such sub-tidal current variability is typical for tropical lagoons, see Kraines et al. (1998); Taebi et al. (2011).

Using the observed state of the waves and water level outside the reef as forcing functions we have formulated a model for the alongshore flow and water level inside the lagoon. The model is quite simple and can easily be run on ordinary desktop computers, using a modest amount of geophysical data as input. Still our model was able to reconstruct the observed time variability of the currents and water level quite well, including the characteristic dip in the current speed at high tide. This local minimum speed at high tide is usually explained as a reduction in the radiation stress gradient as less wave breaking occur over the reef when the water level is high e.g., Kraines et al. (1998). At Xai-Xai, where the reef is only 20 m wide we explain this current minimum as the increased area available for the outgoing water flux at high tide reducing the speed necessary to maintain the volume flux.

We have found that flushing of the lagoon is very efficient, with renewal time less than one hour. However, if waves are ignored and only the tidal component is considered the flushing time was found to be 16 h. Hence the cross-reef volume flux is dominated by the wave-induced transport.

A two years (2011–2012) simulation has been run using forcing from a tidal model (Egbert and Erofeeva, 2002), and wave climate from ERA-Interim reanalysis. The mean sea level differences become unrealistically high for very strong wave forcing, possibly related to non-linear wave effects.

The timing of the extreme current speed for the two year period has been compared with the frequent drowning casualties occurring at this beach (Fig. 9c), but no relation was found.

Acknowledgements

This study was in part financed through the NOMA-project sponsored by the Norwegian Development Agency NORAD, project number NOMAPRO-2007/10049. We would like to thank the Centro de Desenvolvimento Sustentavel para Zonas Costeiras (CDS-ZC) of the Ministry of Environment in Mozambique for the support provided, and also two anonymous reviewers for constructive remarks and suggestions, which significantly improved the manuscript.

References

Angwenyi, C.M., Rydberg, L., 2005. Wave-driven circulation across the coral reef at Bamburi Lagoon, Kenya. Estuar. Coast. Shelf Sci. 63 (3), 447–454. http://dx.doi.org/10.1016/j.ecss.2004.12.008.

Antuono, M., Brocchini, M., Grosso, G., 2007. Integral properties of the swash zone and averaging. Part 3. Longshore shoreline boundary conditions for wave-averaged nearshore circulation models. J. Fluid Mech. 573, 399–415.

Christensen, K.H., Breivik, O., Gammelsrød, T., Hoguane, A., Furaca da Silva, N.B., Nharreluga, B., Taskjelle, T., Poio, M.V., 2013. Waves and Dangerous Currents at Xai-Xai Beach, Mozambique. Tech. Rep. 17/2013. Norwegian Meteorological Institute.

Dee, D.P., Uppala, S.M., Simmons, A.J., Berrisford, P., Poli, P., Kobayashi, S., Andrae, U., Balmaseda, M.A., Balsamo, G., Bauer, P., Bechtold, P., Beljaars, A.C.M., van de Berg, L., Bidlot, J., Bormann, N., Delsol, C., Dragani, R., Fuentes, M., Geer, A.J., Haimberger, L., Healy, S.B., Hersbach, H., Hólm, E.V., Isaksen, L., Kållberg, P., Köhler, M., Matricardi, M., McNally, A.P., Monge-Sanz, B.M., Morcrette, J.-J., Park, B.-K., Peubey, C., de Rosnay, P., Tavolato, C., Thépaut, J.-N., Vitart, F., 2011. The ERA-Interim reanalysis: configuration and performance of the data assimilation system. Q. J. R. Meteorol. Soc. 137 (656), 553–597. http://dx.doi.org/10.1002/qj.828.

Egbert, G.D., Erofeeva, S.Y., 2002. Efficient inverse modeling of Barotropic Ocean tides. J. Atmos. Ocean. Technol. 19 (2), 183–204. http://dx.doi.org/10.1175/1520-0426(2002)019<0183:EIMOBO>2.0.CO;2.

Gourlay, M.R., 1996. Wave set-up on coral reefs. 1. Set-up and wave-generated flow on an idealised two dimensional horizontal reef. Coast. Eng. 27 (3–4), 161–193. http://dx.doi.org/10.1016/0378-3839(96)00008-7.

Kirugara, D., Cederlöf, U., Rydberg, L., 1998. Wave-induced net circulation in a reef fringed lagoon: Bamburi, Kenya. Ambio 27 (8), 752–757. http://www.jstor.org/stable/4314826.

Kraines, S.B., Yanagi, T., Isobe, M., Komiyama, H., 1998. Wind-wave driven circulation on the coral reef at Bora Bay, Miyako Island. Coral Reefs 17 (2), 133–143. http://dx.doi.org/10.1007/s003380050107.

Longuet-Higgins, M.S., 1953. Mass transport in water waves. Philos. Trans. R. Soc. Lond. Ser. A Math. Phys. Sci. 245 (903), 535–581. http://dx.doi.org/10.1098/rsta.1953.0006.

Lowe, R.J., Falter, J.L., Monismith, S.G., Atkinson, M.J., 2009. A numerical study of circulation in a coastal reef-lagoon system. J. Geophys. Res. 114 (C6), C06022. http://dx.doi.org/10.1029/2008JC005081.

Lowe, R.J., Hart, C., Pattiaratchi, C.B., 2010. Morphological constraints to wave-driven circulation in coastal reef-lagoon systems: a numerical study. J. Geophys. Res. Oceans 115 (C9). http://dx.doi.org/10.1029/2009JC005753 n/a–n/a.

Marshall, J., Plumb, R.A., 2008. Atmosphere, Ocean and Climate Dynamics: an Introductory Text. In: No. 93 in International Geophysical Series. Academic Press.

Munk, W.H., Sargent, M.C., 1954. Adjustment of Bikini Atoll to Ocean Waves. In: Geological Survey Professional Paper, vol. 260-D, pp. 275–280.

Prager, E.J., 1991. Numerical simulation of circulation in a Caribbean-type backreef lagoon. Coral Reefs 10 (4), 177–182. http://dx.doi.org/10.1007/BF00336771.

Sete, C.I., Ruby, J., Dove, V., 2002. Seasonal Variation of Tides, Currents, Salinity and Temperature along the Coast of Mozambique. Tech. rep.. Instituto Nacional de Hidrografia e Navegacao, Maputo http://hdl.handle.net/1834/188.

Sibul, O., 1955. Flow over reefs and structures by wave action. Trans. Am. Geophys. Union 36, 61–71. http://dx.doi.org/10.1029/TR036i001p00061.

Stockdon, H.F., Holman, R.A., Howd, P.A., Sallenger Jr., A.H., 2006. Empirical parameterization of setup, swash, and runup. Coast. Eng. 53 (7), 573–588. http://dx.doi.org/10.1016/j.coastaleng.2005.12.005.

Taebi, S., Lowe, R., Pattiaratchi, C., Ivey, G., Symonds, G., 2012. A numerical study of the dynamics of the wave-driven circulation within a fringing reef system. Ocean Dyn. 62, 585–602. http://dx.doi.org/10.1007/s10236-011-0514-4.

Taebi, S., Lowe, R., Pattiaratchi, C., Ivey, G., Symonds, G., Brinkman, R., 2011. Near-shore circulation in a tropical fringing reef system. J. Geophys. Res. 116 (C2), C02016. http://dx.doi.org/10.1029/2010JC006439.

Weber, J.E., Broström, G., Christensen, K.H., 2007. Radiation stress and the drift in gravity waves with Rayleigh friction. In: International Offshore and Polar Engineering, pp. 1994–1999.